Available online at www.sciencedirect.com

ScienceDirect

Proceedings of the Combustion Institute 36 (2017) 2823–2832

Proceedings of the Combustion Institute

www.elsevier.com/locate/proci

Experimental study on turbulent expanding flames of lean hydrogen/air mixtures

J. Goulier [a], A. Comandini [a], F. Halter [a,b], N. Chaumeix [a,*]

[a] *Institut de Combustion, Aérothermique, Réactivité et Environnement (ICARE), CNRS-INSIS, 1C Avenue de la Recherche Scientifique, F-45071 Orléans Cedex 02, France*

[b] *University of Orléans, France*

Received 4 December 2015; accepted 10 June 2016

Available online 23 June 2016

Abstract

The aim of this paper is to report new experimental results on the effect of turbulence on the combustion properties of lean to stoichiometric H_2/air mixtures in a closed, fan-stirred, spherical vessel. To do so, a new experimental setup, spherical bomb, has been used to investigate the effect of a given and well-characterized turbulence intensity on the increase of hydrogen/air flame speed and on the combustion pressure. The initial hydrogen molar percent of H_2 in air was comprised between 16% and 28%. The initial turbulence created in the vessel prior to ignition was varied between 0.56 and 2.81 m/s for an integral length scale of around 50 mm. It was shown that the turbulent speed increases drastically when the turbulence is increased but the maximum combustion pressure remains the same. A correlation was proposed in order to the turbulent speed. The proposed turbulent flame speed correlation was able to predict not only the present data but also the results of the literature (Kitagawa et al., 2008).

Keywords: Turbulent flame; Hydrogen flame; Expanding flames; Hydrogen safety

1. Introduction

As demonstrated during the March 2011 severe nuclear accident in Fukushima, Japan, accumulation and subsequent combustion of hydrogen gas produced by an overheated nuclear core reacting with steam can breach a reactor's containment structures and result in widespread radioactive contamination. The assessment of the hydrogen risk is based on the use of codes using models beforehand validated in particular for the simulation of pressure and temperature loadings resulting from the combustion of hydrogen. Several hydrogen deflagration benchmark exercises [1,2] have concluded that the models used are able of reproducing the pressure peaks generated by the combustion process. However, flame speed maximum values were generally over predicted indicating limitations in combustion models. This phase should absolutely be correctly simulated knowing that the turbulent propagation is a key phase before a possible transition to detonation, which possibly occurred in the reactor 3 in Fukushima.

In this context, the configuration of expanding turbulent flames is of great interest. However, while

* Corresponding author. Fax: +33 2 38 69 60 04.
E-mail address: chaumeix@cnrs-orleans.fr (N. Chaumeix).

http://dx.doi.org/10.1016/j.proci.2016.06.074
1540-7489

there is a clear relation between the propagation speed of a laminar flame front and its stretch rate, the acceleration mechanism of turbulent expanding flames is more complex. Several scaling laws for normalized turbulent flame speeds have been experimentally obtained [3,4]. In particular, in [3], turbulent propagation speeds normalized by the laminar counterpart ($V_T/V_L{}^0$) follow a scaling law based on the square root of a modified Reynolds number, irrespective of the fuel, equivalence ratio, pressure and turbulence intensity. However, this relation is only valid for positive Markstein lengths, where lean hydrogen/air mixtures present negative Markstein lengths.

Most of past studies [3–14], even for hydrogen flames [15], were performed at relatively reduced scales. Chamber equivalent diameters spans between 58 mm [11] to 406 mm [15] with most of the diameters between 200 and 300 mm [5,8–10,13]. Several authors noticed that the turbulent burning velocity extracted from flame front evolutions continually increased during the combustion process. Two mains reasons may be advanced. First, after its central ignition, the flame expands and is wrinkled by imposed turbulence. Its hydrodynamic scales are also increased. Secondly, the flame response time may be of the order of turbulent time scales, inducing unsteadiness in flame response. To overcome these limitations, the size of investigation should be large enough to reach a steady state. Subsequently, a large experimental rig has been developed with an internal diameter of 563 mm allowing flame visualization till a maximal radius of 70 mm.

The present study has two major motivations. First, we will assess the turbulence effect on the propagation of expanding hydrogen/air flames in terms of pressure evolution and turbulent burning velocities. Second, we will take advantage of the large dimensions of the rig to investigate the flame response over a large flame radius domain and to discuss the existing scaling laws.

2. Experimental set-up and methodology

2.1. Experimental rig

The experimental set-up consists of two concentric stainless steel spheres. The inner combustion spherical combustion chamber has an inner diameter of 563 mm and a thickness of 42 mm. The outer sphere has an inner diameter of 640 mm and a thickness of 4 mm. A thermal fluid flows between the two spheres for raising the chamber temperature up to 573 K and to maintain this temperature uniform. The chamber was tested at a maximal pressure of 300 bar. For this study, all experiments were performed at a temperature of 293 K.

To allow optical flame visualization, the rig is equipped with four windows (200 mm optical diameter) on the equatorial plane. The initial temperature prior to ignition is measured via 2 thermocouples (±1.5 K). Fresh gases are introduced successively into the chamber, previously vacuumed. The composition of the mixture is thus calculated knowing the partial pressure corresponding to each introduced gas. The residual partial pressure within the chamber after the pumping operation is below 10 Pa. A high precision capacitance manometer is used with accuracy of ± 0.1 Torr. The maximum relative error on the mole fractions of hydrogen, oxygen and equivalence ratio, ϕ, is 0.8%, 0.07 % and 1.8%, respectively.

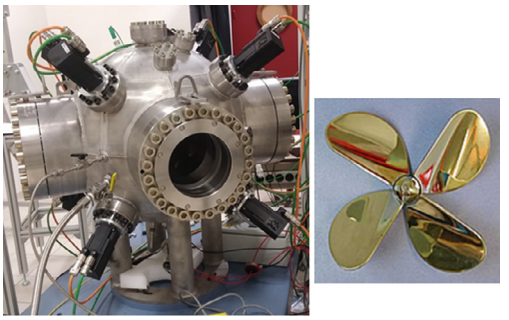

Fig. 1. View of the spherical bomb with its equipment and of the fan used in the turbulent experiments.

The fans are located at the vertices of a cube inscribed in a sphere equivalent to the inner chamber diameter. The maximum speed for fans that can be achieved is 10,000 rotations per min (rpm). The propellers geometry was chosen according to Ravi et al. [9] review: a curved shape is chosen for a more intense turbulence while being homogeneous and isotropic. The propellers were 130 mm in diameter four-bladed (55 mm long and 40 mm wide). They are curved with an angle of 45° to the base at an angle of 30° at the blade tip. The blades are oriented to the left and the rotation is in the clockwise direction so that the air is sucked through the propeller. A view of the system is given in Fig. 1.

Two tungsten electrodes are mounted along a diameter of the sphere, in the horizontal plane. They are linked to a high voltage discharge in order to create the electric spark necessary to ignite the mixture. The electric spark is used to trigger the recording equipment (camera and oscilloscopes) in order to synchronize the temporal flame growth with the evolution of the pressure inside the bomb. Indeed, the temporal behavior of the induced overpressure following the ignition is measured with two fast piezoelectric pressure transducer (Kistler 6001 and 601A models).

2.2. Flame visualization

The flame propagation visualization is done using a Schlieren imaging device (Z type) coupled with ultra-fast camera. This system is mainly

composed of a 300 W Lot-Oriel xenon lamp, a pair of concave spherical mirrors of 1.50 m focal length and a screen. The projection of the image of the flame contours on a screen is recorded by an ultra-fast camera (Vision Research Phantom V1210; 768 pixels^2; frame rate = 19 kHz).

The binarization procedure is performed on the subtracted flame by applying a threshold to the gray level of the image. A set of morphological filters is then applied to the binarized image resulting in a filtered image. Both the flame surface (Af) and contour are extracted from this filtered image. The flame radius (R_f) considered is inferred from the total flame surface $R_f = \sqrt{Af/\pi}$.

To perfectly control the initial conditions (pressure, temperature and mixture fractions), the overall sequence including both vacuum and filling procedures lasts around one hour. For each conditions presently investigated, ten identical trials were performed. This number may be considered low statistically speaking but it is important to notice that the achieving of all experimental conditions still requires more than two hundred hours.

2.3. Experimental conditions

2.3.1. Turbulent flow prior to ignition

The turbulent flow was fully characterized in previous works using Particle Imaging in non-reactive conditions [16]. It was particularly shown that the fans generated homogeneous and isotropic turbulence in a central area of 100 mm in diameter. The turbulent flow can be notably characterized by its turbulence intensity, measured by the turbulent root-mean-square (rms) velocity u', and by the integral longitudinal length scale L_T. As in [6,11–13], the turbulence intensity was found to be proportional to the rotational fan speed and the integral length scale L independent of the fan speed. Figure 2 illustrates the dependence of the turbulent intensity with the rotational speed from 1000 to 5000 rpm. The root-mean-square values, *Urms* and *Vrms*, of the turbulent fluctuations were evaluated over a 50 mm radius circle (centered on the electrode gap) and are almost equivalent for the whole set of rotation speeds. The low magnitude of the mean velocities, *Umean* and *Vmean*, illustrated the absence of flow, accentuated when compared to the turbulent fluctuations.

The maximal rotational speed set up in the current study was of 4000 rpm. The corresponding fluctuating velocity is of 2.81 m/s. This value is substantial and equivalent to those encountered in previous studies. However, we can stress up that this relative high value is homogeneous over a 50 mm radius circle.

The longitudinal and lateral integral lengths scales were determined based on the spatial correlation coefficients from the velocity fluctuations. Their values at 3000 rpm are respectively of 53 and 37 mm. The rotational speed does not impact significantly these scales. Turbulence details are given in Table 1.

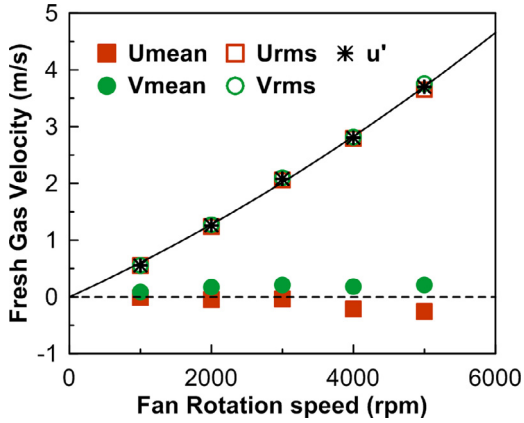

Fig. 2. Turbulent fluctuations and mean velocities (evaluated over a 50 mm radius circle) evolutions with the rotational fan speed.

2.3.2. Experimental conditions

Four different hydrogen concentrations were selected for this study: 16%, 20%, 24% and 28% of hydrogen in the mixture with air, corresponding to equivalence ratios, ϕ, of 0.45, 0.6, 0.65 and 0.97, respectively. All the experiments were performed at $P_{ini} = 100$ kPa and $T_{ini} = 293$ K.

For each concentration, five rotational speeds were tested (0, 1000, 2000, 3000 and 4000 rpm). Turbulence and flame information are summarized in Table 1 for the whole set of conditions. Laminar information was calculated using the thermodynamic equilibrium Cosilab® software and the Mével et al. mechanism [17]. Lewis numbers were evaluated using the methodology proposed by Bechtold et al. [18].

3. Results and discussion

3.1. Combustion regimes

The turbulent combustion regimes encountered in the vessel can be characterized using the Borghi diagram [19]. The operating conditions presented in Table 1 are reported in Fig. 3. These conditions correspond mainly to the flamelet regime. The flamelet concept views the turbulent flame as an ensemble of thin and locally laminar flamelet structures embedded within the turbulent flow field [20].

Only the leanest condition exhibits Karlovitz values above unity. Even if these flames still should belong to the flamelet regime, based on the direct simulations of Poinsot et al. [21], they will certainly be heavily wrinkled. Flame visualizations are

Table 1
Turbulence and flame information for the investigated experimental conditions. xH_2: hydrogen molar fraction, S_L^0: laminar burning velocity, δ_{therm} flame thickness based on temperature profile, Le: Lewis number, u': fluctuating velocity, Ka: Karlovitz number, Da: Damköhler number, Re_T: Turbulent Reynolds number.

xH_2	u' (m/s)	L_T (mm)	S_L^0(m/s)	$\delta_{(gradT)max}$ (mm)	$Le_{effec.}$	u'/S_L^0	Ka	Da	Re_T
0.16	0.56 ± 0.01	43.9 ± 3.1	0.46 ± 0.02	0.523	0.458	1.22	0.22	30.6	45.1
	1.26 ± 0.03	49.0 ± 3.5				2.76	0.70	15.1	113.5
	2.08 ± 0.04	53.0 ± 2.7				4.50	1.42	10.0	201.6
	2.81 ± 0.03	52.4 ± 1.4				6.15	2.27	7.3	270.9
0.20	0.56 ± 0.01	43.9 ± 3.1	0.92 ± 0.03	0.382	0.561	0.61	0.06	105.0	38.9
	1.26 ± 0.03	49.0 ± 3.5				1.38	0.19	51.8	98.1
	2.08 ± 0.04	53.0 ± 2.7				2.25	0.39	34.2	174.1
	2.81 ± 0.03	52.4 ± 1.4				3.08	0.62	24.9	234.0
0.24	0.56 ± 0.01	43.9 ± 3.1	1.41 ± 0.05	0.351	0.712	0.40	0.03	211.8	33.4
	1.26 ± 0.03	49.0 ± 3.5				0.90	0.09	104.6	84.2
	2.08 ± 0.04	53.0 ± 2.7				1.47	0.18	69.0	149.5
	2.81 ± 0.03	52.4 ± 1.4				2.01	0.28	50.2	201.0
0.28	0.56 ± 0.01	43.9 ± 3.1	1.93 ± 0.03	0.350	0.956	0.29	0.02	331.9	28.1
	1.26 ± 0.03	49.0 ± 3.5				0.66	0.05	163.8	70.7
	2.08 ± 0.04	53.0 ± 2.7				1.07	0.10	108.2	125.6
	2.81 ± 0.03	52.4 ± 1.4				1.47	0.17	78.6	168.8

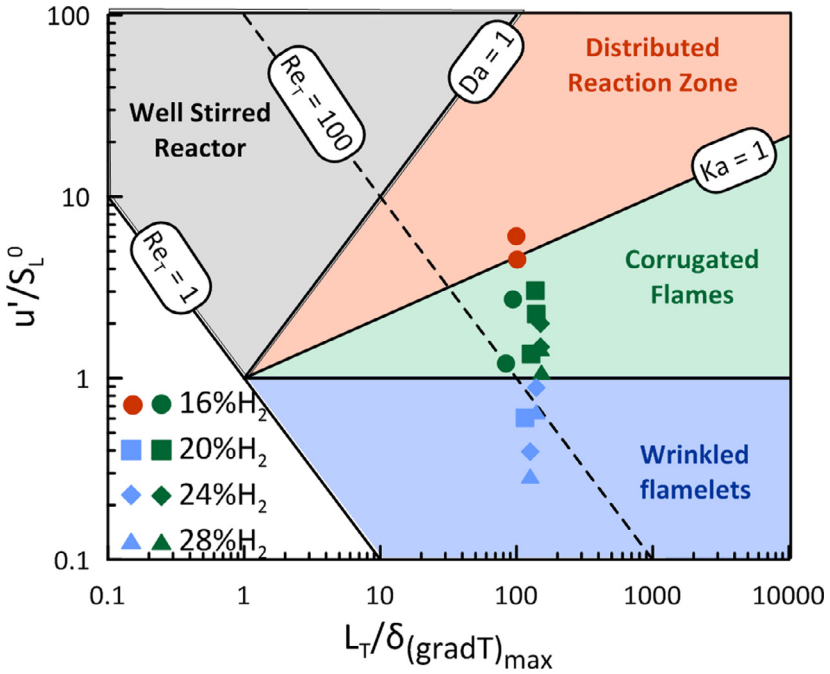

Fig. 3. Experimental conditions reported in the turbulent combustion diagram.

reported in Fig. 4. In the left column, flame visualizations obtained in a quiescent medium are presented to better emphasize turbulent effects.

One can notice that even for a large flame radius of 60 mm, the flame maintains a spherical geometry reinforcing the quality of the turbulent flow. For all the mixtures considered, the turbulence level increase significantly modifies the flame structure. For $\phi = 0.45$, the flame is highly wrinkled even for a non-turbulent regime. The flame front surface is impacted by thermo-diffusive instabilities linked to the high molar diffusivity of hydrogen. When u' is increased, the flame structure is slightly modified. However, for the highest turbulence condition (4000 rpm), one can clearly see a change in the flame morphology, maybe due to the occurrence of local extinctions as also reported by Wu et al. [22].

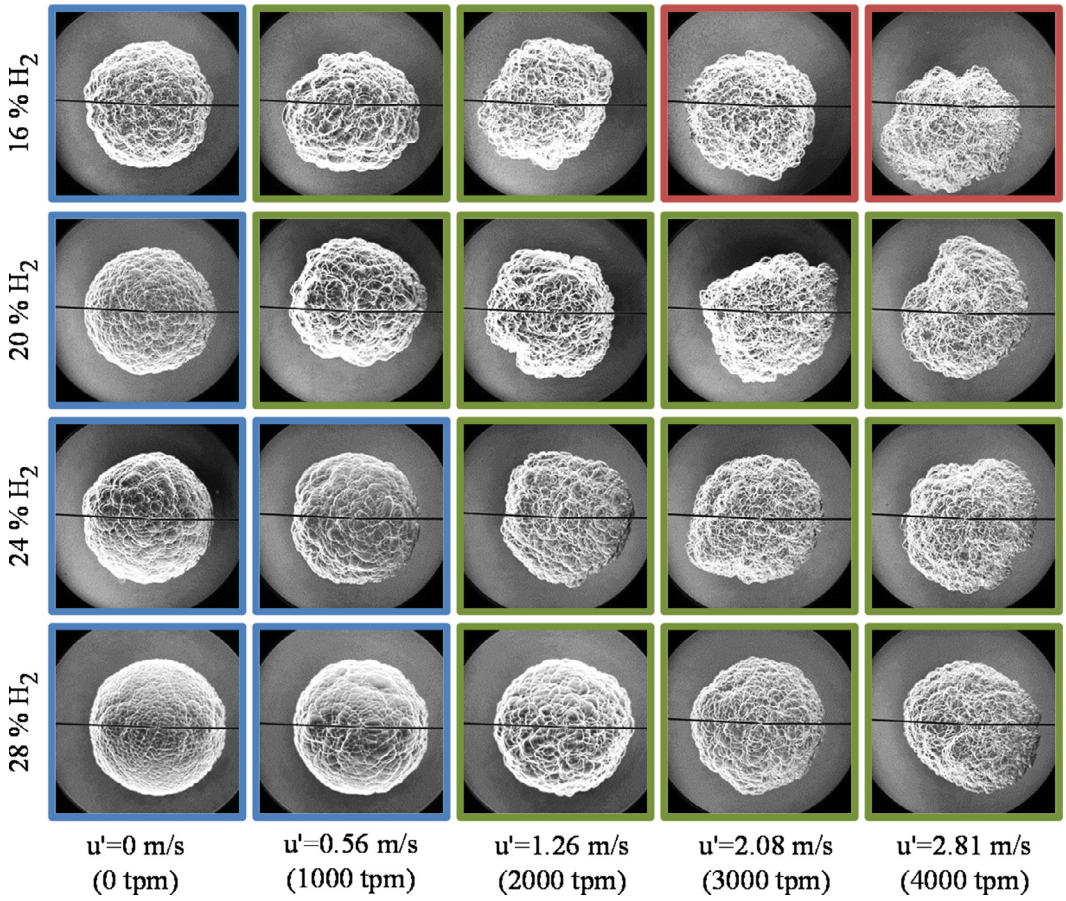

Fig. 4. Flame images with a mean radius of 60 mm. $P_{ini} = 100$ kPa, $T_{ini} = 293$ K.

3.2. Turbulence effect on pressure evolution

The temporal behavior of the induced overpressure following the ignition is measured with two fast piezoelectric pressure transducer (Kistler 6001 and 601A models). They are mounted flush with inner wall of the vessel and located on opposite sides along a diameter of the bomb at +42° and −42° from the equatorial plan respectively. The evolution of the pressure inside the spherical vessel is strongly affected by the presence of the initial turbulence. The total volume of the fresh gases is combusted in a much shorter time. However, the maximum overpressure reached at the end of the combustion is rigorously identical for all levels of turbulence (4.7 bar in this case). Over pressure traces measured by the pressure transducer located in the lower part of the chamber are reported in Fig. 5 for the leanest case ($\phi = 0.45$) and different fan speeds.

The maximum pressure, $P_{max,exp}$, reached does not vary with the turbulence level when the hydrogen content varies from 16% to 28% in air. The

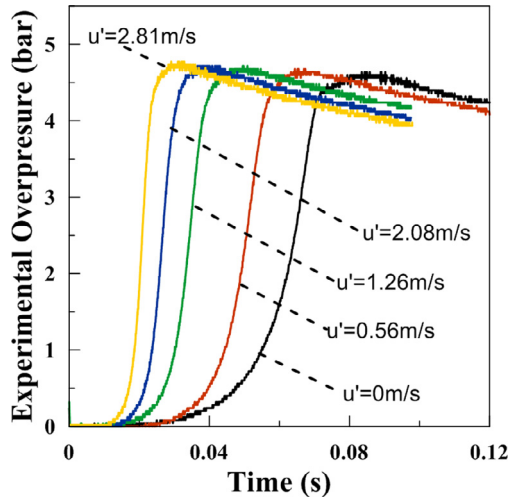

Fig. 5. Overpressure traces measured by the pressure transducer located in the lower part of the chamber. Hydrogen/air $\phi = 0.45$. $P_{ini} = 101$ kPa and $T_{ini} = 293$ K.

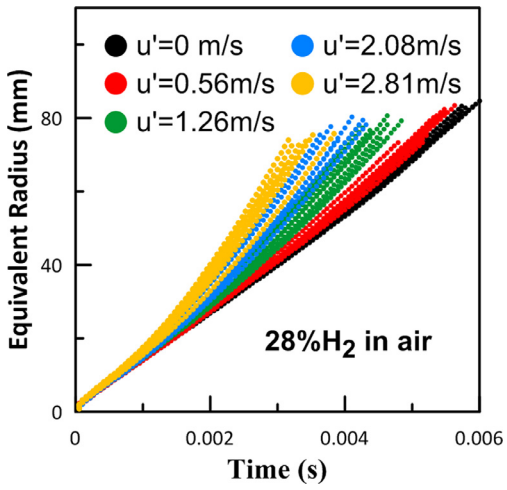

Fig. 6. Impact of the fluctuating velocity on flame radius for different hydrogen percentages. $P = 101$ kPa, $T = 293$ K.

standard deviation is small compared to the measured value. However, the time interval between the start of ignition ($t = 0$ s) and $P_{max,exp}$ substantially decreases as u' increases.

The measured $P_{max,\,exp}$ is compared to the value of the pressure for a complete and adiabatic combustion (P_{AICC}) estimated using the thermodynamic equilibrium Cosilab® software with the species involved in the Mével et al. mechanism [17]. The ratio P_{max}/P_{AICC} is close to 0.96 in the absence of initial turbulence for all investigated conditions and increases by less than 1% when the initial mixture is turbulent.

3.3. Turbulent flame speed

The evolution of the flame radius as a function of time is given in Fig. 6 for different conditions. Several experiments have been performed for each level of initial turbulence. As the turbulence level increases, the spread of the measured radius profile versus time is larger. It is then mandatory to perform several experiments to have a more meaningful average.

In case of expanding flames, turbulent propagation speed V_T is defined as the time derivative of the turbulent flame radius (R_f). Several studies have evaluated V_T at a given mean flame front radius R_0 [10,15,23,24]. In other studies [3–5,14], V_T evolution was interpreted either with time or R_f. The latest approach seems to be more relevant to account of the unsteadiness in flame response. Each experimental condition was repeated at least ten times. For sake of clarity, only the average profiles will be discussed. In Fig. 7, two confidence intervals corresponding to 95% and 50% of confidence have also been added. The 95% confidence interval corresponds to the darkest area. This figure corresponds to the richest case ($\phi = 0.97$). To better point out turbulence effects, the quiescent condition impacted by hydrodynamic and thermo-diffusive instabilities is also reported (black solid line). The theoretical flame speed corresponding to a smooth flame, labeled $V_{S,\,smooth}$, is also plotted (purple solid line).

V_T increases notably with u'. The velocity increase induced by thermo-diffusive instabilities is limited compared to turbulent effects. As the turbulence in the vessel is spatially homogeneous and isotropic, one could expect V_T to tend towards a constant value when R_f increases. However, it still increases throughout flame propagation. The same behavior is reported by [15] for hydrogen/air mixtures for similar initial conditions and flame size. Previous studies [3–5] have attempted to explain the acceleration of expanding turbulent flames as a consequence of the extending turbulence spectra affecting the flame front as the flame grows. Since Abdel-Gayed et al. [5] study, it is well-known in the literature that the initial small flame front is not exposed to the full spectrum of turbulence. It is first affected only by the smallest eddies (smaller than the flame size) which can corrugate the flame front, while the largest ones have only a kinematic effect on the flame kernel and might convect it [7,25]. In other words, as the flame size grows, the turbulent flame will self-accelerate due to the expansion of the spectrum of perturbations to larger wavelengths. Bradley et al. [7] assume that the maximum wavelength that can wrinkle a flame corresponds to the flame diameter. Thus, the acceleration of the turbulent flame in the early stages of flame propagation should cease when the flame length scale R approaches the flow turbulent length scale, at which the growth of the spectrum is terminated. In our experiments, the largest length scale characterizing the turbulent flow is the integral length scale, which has been previously found independent of the rotational fan speed, has been evaluated at $L = 52$ mm. This is not in agreement neither with our experimental results nor with the literature [3,4,15].

The most recent scaling laws proposed [3,4] embed the flame radius information. Consequently, they should be able to reproduce this increase. Chaudhuri et al. [3] correlation was compared to our results (from 16% to 28% of H_2 in air) for R_f up to 70 mm (Fig. 8). This correlation captures the shape of V_T/V_s^0 versus R_f. This correlation relies on the Markstein length, L_b, as the scaling factor for the flame radius, R_f. In the present conditions, L_b decreases as x_{H_2} is increased: it is equal to -1.19, -0.42, -0.21 and $+0.20$ mm for $x_{H_2} = 16\%$, 20%, 24% and 28% respectively. Hence the absolute value of L_b used in the Chaudhuri correlation decreases with the hydrogen molar percent. But, this correlation was based on a limited maximal flame radius of 20 mm and for mixtures with large positive L_b.

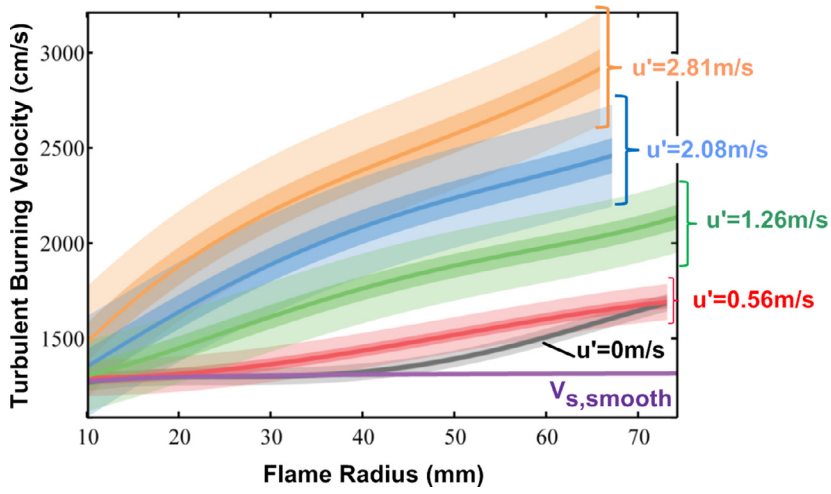

Fig. 7. Experimental Turbulent burning velocities as a function of flame radius for different turbulence conditions. 28% of hydrogen ($\phi = 0.97$). $P = 101$ kPa and $T = 293$ K.

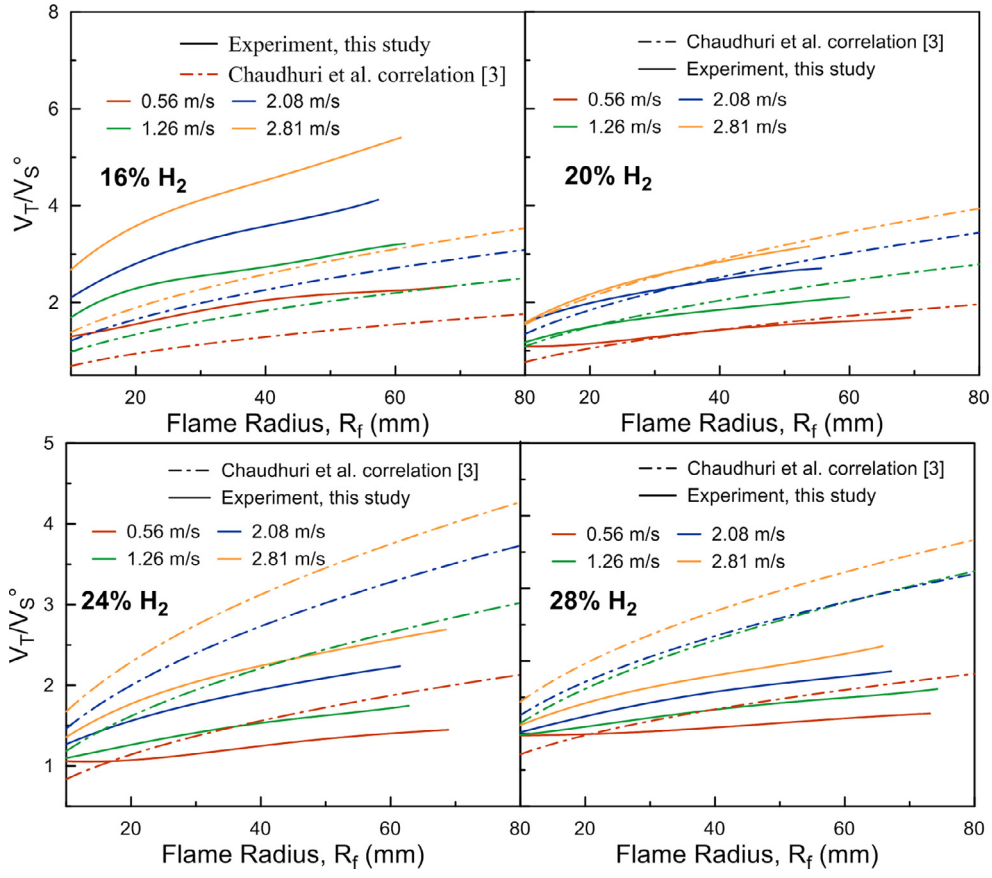

Fig. 8. Evolution of the normalized speed versus the flame radius for different H_2/air mixtures and for different u'. Comparison with the correlation of [3].

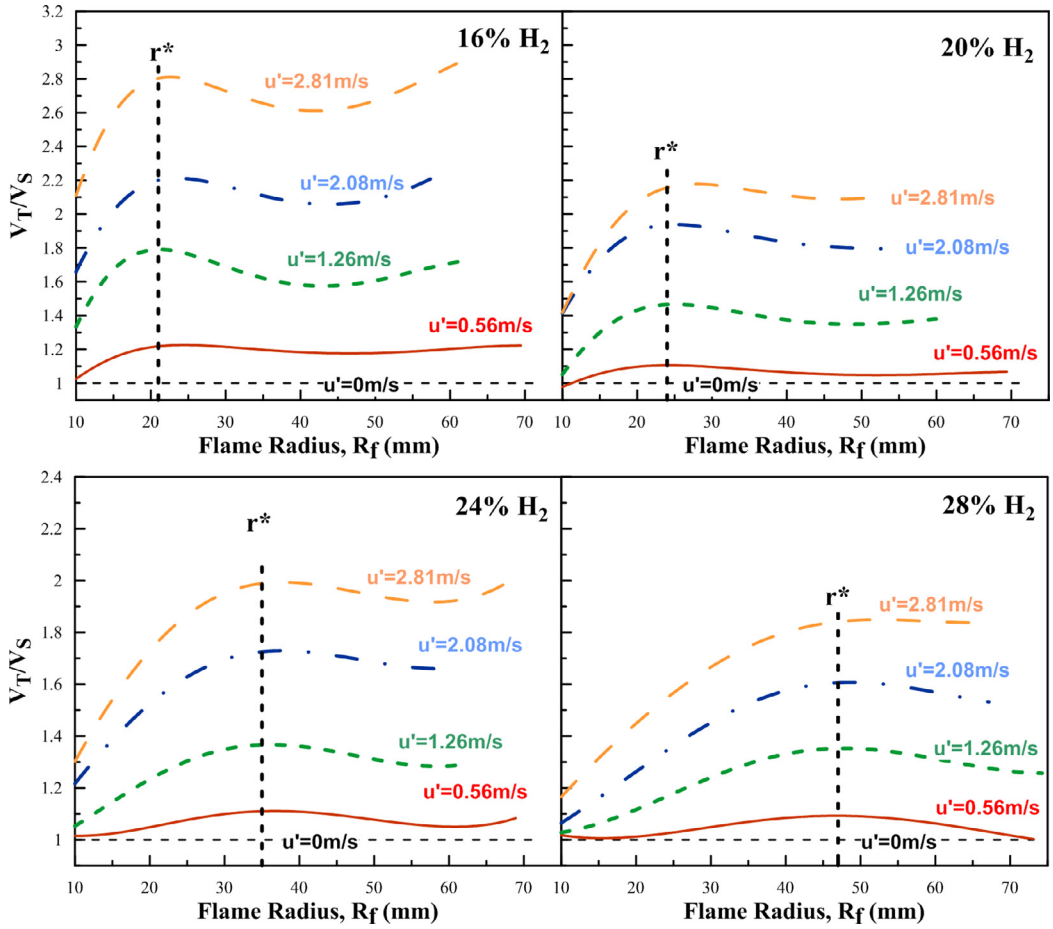

Fig. 9. Evolution of the normalized turbulent flame speed, V_T/V_S, $u' = 0$, versus the flame radius. $P = 101$ kPa and $T = 293$ K.

Given the domain of validity of the correlation, the results are fairly reproduced.

To account of the intrinsic wrinkling of the flame front induced by thermodiffusive and Darrieus–Landau instabilities, V_T was normalized by the speed obtained for the quiescent condition ($u' = 0$), $V_{S,u'=0}$. The normalization has been performed based on the radius of the flame and not on the time. Results are reported in Fig. 9.

Within the observation domain, and for all turbulent conditions, $V_T/V_{S,u'=0}$ initially increases up to a maximum value for a critical flame radius (noted r^* on the figure). Above this critical radius, the flame speed decreases slightly before increasing again. However, due to the domain size this second increase could only be guessed from the shape of the curves. The value of r^*, although variable, is of the order of magnitude of L_T. The variability may be explained by the variable occurrence of the flame instabilities [25] for the different x_{H_2}. After this value, the normalized velocities exhibit a plateau synonymous with a stabilization of the flame velocity and so the flame structure. The initial phase of the flame propagation corresponds to the unsteady phase, usually observed with smaller experimental set-ups.

A new correlation ($R^2 = 0.902$) is proposed based on these new experimental results applicable to lean hydrogen/air mixtures relevant to nuclear safety assessment:

$$\frac{V_{S,T}}{V_S^0} = (1.61 \pm 0.01) \cdot \left(\frac{r}{L_T}\right)^{0.333\pm0.002} \times \left(\frac{u'}{S_L^0}\right)^{0.526\pm0.002} (\mathrm{Le})^{-0.140\pm0.005} \quad (1)$$

This correlation was able to reproduce our data as well as the results of Kitagawa et al. as it is shown in Fig. 10.

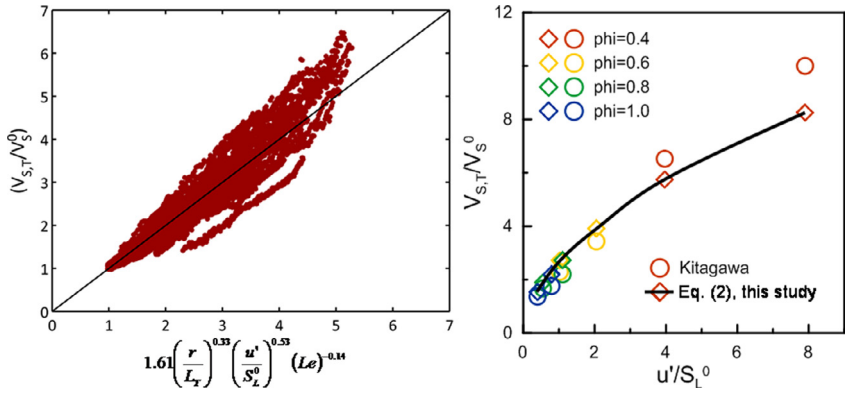

Fig. 10. Comparison between the experimental V_T/V_s^0 and Eq. (1) predictions. (a) This study, (b) Kitagawa et al. [15] study.

4. Conclusion

This study presented new results concerning turbulent flame speed and combustion overpressure of lean to nearly stoichiometric H_2/air mixtures obtained in a new facility designed and built at our laboratory, CNRS-ICARE. The setup consists of a spherical bomb equipped with 8 fans that are mounted symmetrically along the inner wall of the bomb. It was demonstrated we were able to produce a large volume (around 100 mm in radius) inside the spherical vessel where the turbulence is indeed homogeneous and isotropic with intensities that varied from 0.57 m/s up to 2.81 m/s. With this new facility, the turbulent flame speed of lean mixtures of hydrogen/air mixtures with hydrogen molar percent between 16% and 28% were determined. A correlation between turbulent speed and turbulent integral scale was proposed that was able to describe not only the present data but also data from the literature. This correlation will be used to improve safety analyses of CFD code predictions of flame acceleration level for lean H_2/air mixtures in ENACCEF [1].

Acknowledgments

The authors acknowledge the financial support of the CNRS and the IRSN (Contrat CNRS-IRSN 07-2653) (France).

Supplementary materials

Supplementary material associated with this article can be found, in the online version, at doi: 10.1016/j.proci.2016.06.074.

References

[1] A. Bentaib, A. Bleyer, N. Meynet, et al., *Ann. Nucl. Energy* 74 (2014) 143–152.
[2] W. Breitung, S. Dorofeev, A. Kotchourko, et al., *Nucl. Eng. Des.* 235 (2–4) (2005) 253–270.
[3] S. Chaudhuri, F. Wu, C.K. Law, *Phys. Rev. E* 88 (3) (2013) 033005.
[4] S. Chaudhuri, F. Wu, D. Zhu, C.K. Law, *Phys. Rev. Lett.* 108 (4) (2012) 044503.
[5] R.G. Abdel-Gayed, K.J. Al-Khishali, D Bradley, *Proc. R. Soc. Lond. A: Math. Phys. Eng. Sci.* 391 (1801) (1984) 393–414.
[6] D. Bradley, M.Z. Haq, R.A. Hicks, et al., *Combust. Flame* 133 (4) (2003) 415–430.
[7] D. Bradley, M. Lawes, M.S. Mansour, *Combust. Flame* 158 (1) (2011) 123–138.
[8] T.D. Fansler, E.G. Groff, *Combust. Flame* 80 (3–4) (1990) 350–354.
[9] S. Ravi, S. Peltier, E. Petersen, *Exp. Fluids* 54 (1) (2012) 1–16.
[10] S.S. Shy, W.K. I, M.L. Lin, *Exp. Therm. Sci.* 20 (3–4) (2000) 105–114.
[11] V. Sick, M.R. Hartman, V.S. Arpaci, R.W. Anderson, *Combust. Flame* 127 (3) (2001) 2119–2123.
[12] M. Weiß, N. Zarzalis, R. Suntz, *Combust. Flame* 154 (4) (2008) 671–691.
[13] B. Galmiche, N. Mazellier, F. Halter, F. Foucher, *Exp. Fluids* 55 (1) (2013) 1–20.
[14] S. Chaudhuri, A. Saha, C.K. Law, *Proc. Combust. Inst.* 35 (2) (2015) 1331–1339.
[15] T. Kitagawa, T. Nakahara, K. Maruyama, K. Kado, A. Hayakawa, S. Kobayashi, *Int. J. Hydrog. Energy* 33 (20) (2008) 5842–5849.
[16] J. Goulier, N. Chaumeix, F. Halter, N. Meynet, A. Bentaïb, *Nucl. Eng. Des. J.* (submitted for publication).
[17] R. Mével, F. Lafosse, N. Chaumeix, G. Dupré, C.E. Paillard, *Int. J. Hydrog. Energy* 34 (21) (2009) 9007–9018.
[18] J.K. Bechtold, M. Matalon, *Combust. Flame* 127 (1–2) (2001) 1906–1913.

[19] R. Borghi, D. Escudie, *Combust. Flame* 56 (2) (1984) 149–164.
[20] N. Peters, *Symp. (Int.) Combust.* 21 (1) (1988) 1231–1250.
[21] T. Poinsot, D. Veynante, S. Candel, *Symp. (Int.) Combust.* 23 (1) (1991) 613–619.
[22] F. Wu, A. Saha, S. Chaudhuri, C.K. Law, *Proc. Combust. Inst.* 35 (2) (2015) 1501–1508.
[23] M. Fairweather, M.P. Ormsby, C.G.W. Sheppard, R. Woolley, *Combust. Flame* 156 (4) (2009) 780–790.
[24] C. Mandilas, M.P. Ormsby, C.G.W. Sheppard, R. Woolley, *Proc. Combust. Inst.* 31 (1) (2007) 1443–1450.
[25] V.Y. Akkerman, S. Chaudhuri, C.K. Law, *Phys. Rev. E* 87 (2) (2013) 023008.